High-speed deposition of graphite-like carbon film by Ar/C_6H_6 surface-wave plasma with high-voltage pulse biasing

Hansin Bae[1], Kensuke Sasai[2], Haruka Suzuki[1,2], and Hirotaka Toyoda[1,2,3]

[1]*Department of Electronics, Nagoya University, Furo-cho, Chikusa-ku, Nagoya 464-8603, Japan*

[2]*Center for Low Temperature Plasma Sciences, Nagoya University, Furo-cho, Chikusa-ku, Nagoya 464-8603, Japan*

[3]*National Institute for Fusion Science, 322-6, Oroshi, Toki, 509-5292 Japan.*

Abstract

A method for graphite-like carbon (GLC) deposition using Ar/C_6H_6 surface-wave plasma (SWP) is proposed. Characteristic of the SWP, *i,e,* high plasma density with wide spatial uniformity realized uniform carbon film deposition at high deposition rates. To increase sp^2 ratio in carbon films, a pulsed negative bias voltage up to ~2 kV is applied to a substrate. Conductive carbon films of low sheet resistances below ~10^2 Ω/sq is achieved at high deposition rates up to ~6 nm/s with good spatial uniformity (±5%) in an area of ~18×3 cm^2. Film structure is evaluated by Raman spectroscopy, Fourier-transform infra-red spectroscopy, X-ray diffraction, X-ray photoelectron spectroscopy, scanning transmission electron microscopy and electron energy loss spectroscopy. At high negative bias voltages, sp^2-rich with reduced hydrogen content of the film is observed.

Keywords:

PECVD, carbon, conductive carbon film, microwave plasma, graphite-like carbon

1. Introduction

Graphite-like carbon film, a carbon film including high ratio of graphite-like structure (sp^2 bond), is attractive material because of its superior properties such as its high electrical conductivity, anti-corrosion, low friction and so on. Because of such excellent properties, various industrial applications using GLC film have been reported in the last several decades.[1-9] To deposit GLC film, various deposition methods have been proposed such as chemical vapor deposition (CVD) [10-15] or physical vapor deposition (PVD) [16-20] and so on. However, these film deposition processes have difficulties in high deposition rate, high electrical conductivity, or uniform film deposition in large area. For example, typical deposition rate reported so far is less than 0.04 nm/s in PVD process [20] and less than 0.001 nm/s in CVD process [10]. These issues make commercialization of the GLC films difficult. Another candidate deposition process for the GLC film deposition is plasma-enhanced chemical vapor deposition (PECVD), which is promising due to its high productivity under low temperature condition.[21-25] Among various plasma sources, surface-wave plasma (SWP) has high plasma density ($\geq 10^{17}$ m^{-3}) with large-area plasma uniformity.[26~30] Such properties enable us to deposit the GLC film at high deposition rate with good deposition uniformity. Kalita *et al.* reported nanographene film growth using the SWP at a deposition rate of 1.1 nm/s.[24] J. Kim *et al*.[28,29] reported wide-area diamond and graphene deposition by the SWP.

To increase the graphite structure in the carbon film, it is known that ion bombardment is effective.[31~35] Change in the film structure by

varying ion bombardment energy has been reported using various film investigation techniques such as Raman spectroscopy, FT-IR, and so on.[31-35] These studies showed the increase of the sp^2 state in deposited carbon films with increasing the ion bombardment energy ($\geq$1.3 keV). To achieve higher deposition rate without reducing higher film conductivity, however, not only high energy ions but also higher ion-flux to the substrate is required. Deposition precursor gas is important from the viewpoint of the deposition rate. Robertson compared carbon film deposition rates with different hydrocarbon molecules and pointed out benzene has the highest deposition rate in hydrocarbon gases due to its lowest ionization potential.[35]

In this study, we demonstrate deposition of the GLC film by PECVD, that enables us to deposit films with higher film deposition rates. For the enhancement of the electrical conductivity of the film, higher ion flux as well as higher ion energy is required. To satisfy such conditions, the high-density SWP with high negative bias voltage source (<2 kV) is used. The SWP also enables us to produce large-area plasma with good spatial uniformity. Spatial profiles of plasma density and film deposition characteristics such as deposition rate, thickness uniformity, electrical conductivity, and film structure are investigated.

2. Experimental setup

Figure 1(a) shows schematic of experimental apparatus. A vacuum vessel of 50 cm in length, 26 cm in width, and 16 cm in height is equipped with a

quartz plate (50×17 m^2) and is evacuated by a dry pump down to a base pressures less than 0.1 Pa. A slot plate with two arrays of 3 slot antennas and a waveguide are attached to the quartz plate. Based on an electromagnetic field simulation, the slot position is optimized to enhance the microwave radiation. The waveguide is terminated with a plunger to control node position of standing wave in the waveguide. In this study, Cartesian coordinates (x, y, z) with its origin on the center of the quartz plate are defined as shown Fig.1(a). Argon gas is introduced into the vessel through a mass flow controller at a flow rate of 65 sccm. Apart from the Argon gas feed, vaporized benzene (C_6H_6) is fed through a gas manifold at z=3 cm toward a water-cooled substrate stage (26×7 cm^2). The center of the stage is located at x=-7.5 cm off center of the vessel and another coordinate (x_2) on the stage surface is introduced with its origin on the stage center. A total pressure is kept at 13 Pa by a conductance valve. Microwave power (2.45 GHz, 1.3 kW) is applied to the waveguide and the SWP is produced in front of the quartz plate. The deposited film tends to produce sp^3 bonds and to be insulative if the ion bombardment is not enough. This results in charging-up of the film surface by positive charge and unipolar arcing on the film surface. Such situation can be avoided by using pulsed DC biasing, where accumulated charge is released during the pulse-off phase. In this study, the stage is negatively biased by a high impulse voltage generator (maximum voltage: -2 kV, pulse frequency: 500 Hz, pulse-on time: 0.2 ms). Hereafter, stage bias voltage (V_B) is indicated by its absolute value. The voltage and current are measured by a high voltage probe and a current probe, respectively. At the

same stage position and the microwave power, the stage current is almost the same irrespective to the bias voltage. Electrically conductive (n-doped) silicon (100) substrate (size: 18×3 cm^2, resistivity: 10.5 Ω·m, sheet resistance: 150 Ω/sq) is placed on the stage surface. Prior to the film deposition, the silicon substrates are cleaned by an ultrasonic cleaner with acetone and are pre-sputtered by Argon plasma for 2 min at V_B=1 kV. After the pre-sputter of substrates, benzene gas at a flow rate of 50 sccm is introduced through the gas manifold, and the film is deposited on the substrate. Film thickness is measured by a step profiler and electrical resistivity is measured by a four-terminal sensing method. The deposited film thickness is ~ 400 nm in all experiments. A distance from the quartz plate to the stage and bias voltage are varied. Film quality is investigated by Raman spectroscopy, Fourier-transform infrared spectroscopy (FT-IR), X-ray diffraction (XRD), X-ray photoelectron spectroscopy (XPS), scanning transmission electron microscopy (STEM) and electron energy loss spectroscopy (EELS).

Spatial profiles of Ar plasma density are measured using wire Langumuir probes made of tungsten (diameter: 0.1 mm, length: 10 mm). Two identical Langmuir probes are moved along the z axis at x=0 cm and along the x-axis at z=8 cm.

3. Results and Discussions

As mentioned above, ion bombardment during the film deposition plays important role to obtain the GLC film. To evaluate the ion flux to the

substrate, bias voltage and current on the stage are measured. Figure 2 shows voltage and current waveforms at V_B=2.0 kV. Just after turning on the pulse at t=0, ringing is observed (<5μs) with a maximum bias voltage and a current of 3.5 kV and 2 A, respectively. After then, steady state voltage and current at 2.0 kV and 0.75 A, respectively, are observed. By turning off the pulse power at t=0.2 ms, a long falling time is observed. This is due to the charge reduction of the power source capacitor by the current flowing from the plasma.

Spatial distributions of the plasma density and the electron temperature are measured by Langumuir probes. In this measurement, C_6H_6 is not introduced to avoid film deposition on the probe surface. Figure 3(a) and (b) show spatial profiles of the plasma densities along z axis at x=0 and along x axis at z=8 cm, respectively. Ar gas pressure and microwave power are 13 Pa and 1.3 kW, respectively. In Fig. 3(a), the plasma density monotonically decreases with increasing the distance from the quartz plate. Such spatial variation of the plasma density is almost similar with other SWPs.[26,27,30] In Fig. 3(b), uniform plasma along x direction at a density of ~ 4.1×10^{17} m^{-3} is observed. Uniformity of electron temperature at T_e~1.4 eV is also confirmed, although not shown in the figure.

To evaluate spatial uniformity of the film deposition rate, carbon film is deposited at a stage position of z=8 cm by introducing the benzene gas. Figure 4 shows spatial profiles of (a) deposition rate and (b) sheet resistance at various bias voltages. Both the deposition rate and the sheet resistance are almost uniform along x_2 direction irrespective of the bias voltage. Figure 5(a)

and (b) show spatially-averaged deposition rate and sheet resistance, respectively, as a function of the V_B. Both the deposition rate and the sheet resistance decrease with increasing in the V_B . At high bias voltages ($V_B \geq 1.5$ kV), measured sheet resistance is lower than that of the silicon substrate. At V_B=2.0 kV, the deposition rate and the sheet resistance are 6 nm/s and 80 Ω/sq, respectively. These results are better than those of previous studies[10-25] and suggest that energetic ions accelerated by the negative bias voltage contribute to the deposition of sp^2-rich GLC film.

From viewpoint of film structure, it is known that the film conductivity is increased by the increase of the sp^2 state, and the ion flux and ion energy play important roles to control the film conductivity.[31-34] Ion current is proportional to the plasma density and, in this study, the plasma density monotonically decreases with increasing the distance from the dielectric plate. To give an insight into the influence of the ion flux to the film conductivity, GLC film is deposited by changing stage position from z=8 to 16 cm. Figure 6 shows (a) stage bias current, (b) deposition rate and (c) sheet resistance of the deposited film with bias voltage V_B=2.0 kV, as a function of the stage position. Stage bias current monotonically decreases with increasing the z position, which is almost similar with the spatial variation of the plasma density (Fig. 3(a)). Deposition rate monotonically decreases with increasing the z position. This is presumably due to decrease of precursor diffusing to the substrate with increasing the distance between the gas feed and the stage. It is also notable that the sheet resistance increases with increasing stage position. As was indicated in fig. 3(a), the plasma

density monotonically decreases with increasing the z position. As is known that ion flux to the substrate is proportional to the plasma density, the plasma density profile of fig. 3(a) means that ion flux drastically decreases with increasing the distance from the quartz plate. Decrease in the film conductivity is due to the decrease in the ion flux, and this also indicates that the importance of the ion flux as well as the ion energy to the film surface for the conductive film deposition.

In addition to the dependence of the film quality on the substrate position, C_6H_6 flow rate ratio was also varied from 25 sccm to 140 sccm at Ar flow rate, total pressure and bias voltage of 65 sccm, 13 Pa. and 2.0 kV, respectively. Deposition rate monotonically increased from 4.6 nm/s to 7.9 nm/s with increasing C_6H_6 flow rate, *i.e.*, partial pressure. However, the film sheet resistance also increased from 76 Ω/sq to 138 Ω/sq. The result suggests that, to reduce the sheet resistance, ion energy deposited to the film should be higher at higher deposition rates.

To elucidate the mechanism of the film conductivity increase, films are evaluated by Raman spectroscopy using visible light at a wavelength of 532 nm. It is known that Raman spectrum of carbon film is composed of two peaks, *i.e.*, G-peak (graphite peak: 1520 ~ 1600 cm^{-1}) and D-peak (disorder peak: 1340 ~ 1380 cm^{-1}), and that G-peak shift and I(D)/I(G) ratio are good indexes to evaluate the film structure.[1,4,6,8,10-25,27,28,32-36] Figure 7(a) shows normalized Raman spectra of deposited films at bias voltages from 0.5 to 2.0 kV. By increasing the bias voltage, increase of the D-peak relative intensity and of G-peak shift to higher wavenumbers are observed.

To evaluate the G-peak position and I(D)/I(G) ratio more precisely, G- and D-peaks are separated with Gaussian curve fitting. Figure 7(b) and (c) show the bias voltage dependence of the G peak position and the I(D)/I(G) ratio, respectively. Both the G-peak position and the I(D)/I(G) ratio monotonically increases with increasing the bias voltage. Ferrari and Robertson[35,36] reported the relation between Raman spectrum and carbon structures (tetrahedral amorphous carbon (ta-C), amorphous carbon (a-C), nanocrystalline graphite (NCG), and graphite) from the viewpoint of the G-peak position and the I(D)/I(G) ratio. Among carbon structures, G-peak shift to lower wavenumber is apparent in the case of a-C and the I(D)/I(G) ratio has its maximum in the case of NCG. From these facts, we can conclude that the deposited film structure changes from a-C to NCG with increasing the bias voltage. This also suggests that increase of the sp^2 composition in the film with increasing the bias voltage and this is qualitatively consistent with the result of Fig. 5(b), *i.e.*, decrease in the sheet resistance at higher bias voltages.

FT-IR is one of convenient techniques to evaluate hydrogen content in the film because C-H bond absorbs infra-red light at wavenumbers from 2800~3200 cm^{-1}.[35,37,38] Figure 8(a) shows the C-H stretching absorption coefficient spectra of carbon films at V_B=0.5-2.0 kV. The peak absorption coefficient monotonically decreases with increasing the V_B. M. Veres *et al.*[37] reported detailed analysis of the C-H absorption spectrum considering vibration modes such as CH_3 sp^3-asymmetric (2873 cm^{-1}), CH_2 sp^3-asymmetric (2928 cm^{-1}), CH_2 sp^2-symmetric (2973 cm^{-1}), CH sp^2-olefin

(3026 cm^{-1}) and CH_2 sp^2-asymmetric (3058 cm^{-1}). The H content in the film is obtained from following equation (2),

$$n_{\mathrm{H}} = A_{\mathrm{s}} \int \frac{\alpha(\nu)}{\nu} d\nu \quad . \qquad (1)$$

Here, ν, α and A_s are wavenumber, absorption coefficient and coefficient of CH absorption, respectively. A_s value is reported as 8.7×10^{20} cm^{-2}.[38] Bias voltage dependence of the H content is shown in Fig. 8(b). Similar to ref. 34, the H content monotonically decreases with increasing the V_B, suggesting the effect of the ion bombardment on the H reduction in the film. At bias voltages above 1.5 kV, the H content is less than 6×10^{21} cm^{-3} which corresponds to the H atomic composition less than ~5%. This shows deposited film mostly consists of carbon atoms at higher V_B.

GLC film composition is evaluated by X-ray photoelectron spectroscopy (XPS). Monochromatized Al Kα is used for excitation source. Electron emission angle is 0°. Ar ion at an energy of 0.5 keV is injected to sample surface with 50° incident angle before XPS analysis. Chamber for XPS measurement is pumped down to pressure 10^{-7} Pa. Figure 9(a) shows XPS wide-range spectrum (binding energy: 200 ~ 1350 eV) for GLC film deposited at a bias voltage of 2.0 kV. From the spectrum, no apparent peak except for carbon is observed. Figure 9(b) shows XPS spectra of the films deposited at bias voltages from 0.5 to 2.0 kV. Each spectrum is composed of 3 peaks, *i.e.*, sp^2 (284.5±0.1 eV), sp^3 (285.3±0.1 eV) and C-O bond (286.5±0.1eV)[20,23,32,40]. These components are also indicated in the figure. The sp^2 bond obviously increases by increasing the bias voltage from Fig. 9(b). Figure 9(c) shows sp^2/sp^3 content ratio as a function of the

bias voltage. The sp^2/sp^3 content ratio monotonically increases from ~1.0 to ~3.1 by increasing the bias voltage. This result is similar trend with that of Raman spectra. From the detailed investigation of C1s XPS peak, monotonic increase of sp^2/sp^3 ratio was observed up to ~3 at V_B=2.0 kV.

In addition to the above film evaluation, film structure was investigated by X-ray diffraction (XRD). Cu Kα radiation is used for XRD analysis. Anode power is 1.2 kW. Incident angle is changed from 0.1° to 5° with 0.1° interval. But no apparent peak was observed both from in-plane and from 2θ methods from 15° to 80°. From the above measurements, conductive carbon film deposited in this study is considered to be sp^2-rich carbon film presumably with sp^2 clusters in the film which has been introduced by Robertson in Ref [35].

To investigate the structure of deposited carbon film at V_B=2.0 kV in more detail, we also performed aberration-corrected scanning transmission electron microscopy (STEM) and electron energy loss spectroscopy (EELS) at an electron beam energy of 200 kV and an EELS energy dispersion of 0.1 eV/channel. The EELS is set to dual EELS mode with zero-loss peak. As shown in Fig. 10(a), there is no distinguished crystal structure from the TEM image. Figure 10(b) shows EELS spectrum of carbon K-edge. The EELS spectrum is close to the graphitized carbon spectrum in Ref.[41]. Figure 10(c) shows mapping of C_K edge sp^2 bonding intensity (284.9±0.7 eV). The white pixels with red arrows in Fig. 10(c) indicate sp^2 clusters in the carbon film. This means that nano-sized sp^2 clusters are distributed in the carbon film. As the result, the carbon film in this study has an amorphous structure with a

large amount of nano-sized sp^2 clusters.

In the previous study of carbon film deposition by ion beam, sp^3 bond become dominant when the carbon ion energy is ~100 eV, and sp^2 bond is increased when the ion energy is higher than 100 eV.[39] This result suggests that sp^2-rich film can be deposited at higher ion energies. In the case of the PECVD of sp^2-rich film, however, hydrogen atoms incorporated in the film also hinders the sp^2-bond formation and ion bombardment is required also for the hydrogen removal from the film. This means that the enhancement of the ion bombardment not only by the ion flux, but also by the ion energy is required for the sp^2-rich film deposition by the PECVD. In this study, the SWP, a high-density microwave plasma, enables us to increase the ion flux to the substrate. From the plasma density n_o and Bohm velocity $u_B=(kT_e/M)^{1/2}$, ion flux Γ_i is evaluated to be

$$\Gamma_i = n_o u_B , \qquad (2)$$

where, k, T_e and M are Boltzmann constant, electron temperature and ion mass, respectively. The ion flux estimated from the plasma density is $1.2\text{x}10^{21}$ $1/m^2s$. Supposing ion incident energy of 1.5 keV, energy deposition flux to the film is ~$2\text{x}10^{23}$ eV/m^2s taking into account the pulse duty ratio. Considering carbon atom deposition flux ($7\text{x}10^{20}$ C/m^2s) evaluated from the deposition rate (~6 nm/s), ion energy deposition per one depositing carbon atom is estimated to be ~300 eV/C, and this energy is much higher than the ion energy to produce sp^3 and the result is consistent with the previous work showing that higher ion energy produces sp^2 bonds rather than sp^3 bonds. In conventional RF plasma sources, plasma density is one or two orders of

magnitude lower than that of the SWP and energy deposition to the surface with a few 100 eV/C cannot be achieved at high deposition rates (~a few nm/s) with bias voltages of a few keV. This is presumably the reason why the GLC is deposited in the combination of the SWP and the high voltage bias power source.

4. Conclusion

In conclusion, GLC film deposition with high speed was studied using surface wave plasma, benzene precursor gas, and high negative bias voltage. Electrically conductive carbon film at sheet resistance less than 80 Ω/sq was deposited at bias voltages above 1.5 kV. High deposition rate (~6 nm/s) with good spatial uniformity in 16 cm along the waveguide direction was confirmed. Deposited films were investigated by Raman spectroscopy, infra-red spectroscopy, X-ray diffraction (XRD), X-ray photoelectron spectroscopy (XPS), scanning transmission electron microscopy (STEM) and electron energy loss spectroscopy (EELS). At higher bias voltages, sp^2-rich carbon film formation was confirmed and this was consistent with the decreases in the sheet resistance. Film has nano-size sp^2 clusters from XRD, TEM and EELS.

Mechanism of the GLC film formation was discussed from the viewpoint of energy deposition per depositing carbon atom. From estimated energy flux (~2×10^{23} eV/m^2s) and depositing carbon flux (~7×10^{20} C/m^2s), energy deposition per one carbon atom was estimated to be ~300 eV, which was high enough to produce sp^2 bonds in the films. This suggested that high density

plasma source and high voltage biasing was effective to deposit GLC films at higher deposition rates.

References

1. J. Guo, X. Chen and C. Wang, Carbon scaffold structured silicon anodes for lithium-ion batteries, J. Mater. Chem. **20** (2010) 5035-5040. https://doi.org/10.1039/C0JM00215A
2. Y. Show, Electrically conductive amorphous carbon coating on metal bipolar plates for PEFC, Surf. Coat. Technol. **202** (2007) 1252-1255, https://doi.org/10.1016/j.surfcoat.2007.07.065
3. Lei Li, Lin-Lin Liu, Xiaowei Li, Peng Guo, Peiling Ke, and Aiying Wang, Enhanced Tribocorrosion Performance of Cr/GLC Multilayered Films for Marine Protective Application, ACS Appl. Mater. Interfaces **10** (2018) 13187-13198 https://doi.org/10.1021/acsami.8b00628
4. T. Fukutsuka, T. Yamaguchi, S. Miyano, Y. Matsuo, Y. Sugie, Z. Ogumi, Carbon-coated stainless steel as PEFC bipolar plate material, J. Power Sources **174** (2007) 199-205. https://doi.org/10.1016/j.jpowsour.2007.08.096.
5. Lajun Feng, Zuoping Wang, Wenning Shen, Effects of complex graphite-like carbon coating on gear vibration noise, Results Phys. **12** (2019) 1495-1499 https://doi.org/10.1016/j.rinp.2019.01.048.
6. C. Chung, S. Chen, P. Chiu, M. Chang, T. Hung, T. Ko, Carbon film-coated 304 stainless steel as PEMFC bipolar plate, J. Power Sources **176** (2008) 276-281. https://doi.org/10.1016/j.jpowsour.2007.10.022.

7. Shengguo Zhou, Gen Liu, Nengwen Ding, Lunlin Shang, Rui Dang, Jingwen Zhang, Improved performances of lithium-ion batteries by graphite-like carbon modified current collectors, Surf. Coat. Technol. **399** (2020) 126150 https://doi.org/10.1016/j.surfcoat.2020.126150.
8. K. Feng, Y. Shen, H. Sun, D. Liu, Q. An, X. Cai, P. K. Chu, Conductive amorphous carbon-coated 316L stainless steel as bipolar plates in polymer electrolyte membrane fuel cells, Int. J. Hydrog. Energy **34** (2009) 6771-6777. https://doi.org/10.1016/j.ijhydene.2009.06.030.
9. Yongxin Wang, Jibin Pu, Jiafan Wang, Jinlong Li, Jianmin Chen, Qunji Xue, Interlayer design for the graphite-like carbon film with high load-bearing capacity under sliding-friction condition in water, Appl. Surf. Sci. **311** (2014) 816-824 https://doi.org/10.1016/j.apsusc.2014.05.172.
10. A.N. Obraztsov, E.A. Obraztsova, A.V. Tyurnina, A.A. Zolotukhin, Chemical vapor deposition of thin graphite films of nanometer thickness, Carbon **45** (2007) 2017-2021, https://doi.org/10.1016/j.carbon.2007.05.028.
11. M. Yudasaka, R. Kikuchi, T. Matsui, H. Kamo, Y. Ohki, S. Yoshimura, E. Ota, Graphite thin film formation by chemical vapor deposition, Appl. Phys. Lett. **64** (1994) 842-844; https://doi.org/10.1063/1.110998
12. J. Sun , N. Lindvall, M. T. Cole, T. Wang , T. J. Booth, P. Bøggild, K.

B. K. Teo, J. Liu, A. Yurgens, Controllable chemical vapor deposition of large area uniform nanocrystalline graphene directly on silicon dioxide, J. Appl. Phys. **111** (2012) 044103
https://doi.org/10.1063/1.3686135

13. D. Noll, P. Hönicke, Y. Kayser, S. Wagner, B. Beckhoff, U. Schwalke, Transfer-Free in situ CCVD grown nanocrystalline graphene for sub-PPMV ammonia detection, ECS J. Solid State Sci. Technol. **7** (2018) Q3108.
https://doi.org/10.1149/2.0171807jss
14. N. Weber, A. Binder, M. Kettner, S. Hirth, R. T. Weitz, Ž. Tomović, Metal-free synthesis of nanocrystalline graphene on insulating substrates by carbon dioxide-assisted chemical vapor deposition, Carbon **112** (2017) 201-207.
https://doi.org/10.1016/j.carbon.2016.11.007.
15. A.N. Obraztsov, A.V. Tyurnina, E.A. Obraztsova, A.A. Zolotukhin, B. Liu, K. Chin, A.T.S. Wee, Raman scattering characterization of CVD graphite films, Carbon **46** (2008) 963-968
https://doi.org/10.1016/j.carbon.2008.03.002.
16. T. Schumann, M. Dubslaff, M.H. Oliveira Jr, M. Hanke, F. Fromm, T. Seyller, L. Nemec, V. Blum, M. Scheffler, J.M.J. Lopes, H. Riechert, Structural investigation of nanocrystalline graphene grown on ($6\sqrt{3} \times 6\sqrt{3}$)R30°-reconstructed SiC surfaces by molecular beam epitaxy, New J. Phys. **15** (2013) 123034
https://doi.org/10.1088/1367-2630/15/12/123034

17. S. K. Jerng, D. S. Yu, Y. S. Kim, J. Ryou, S. Hong, C. Kim, S. Yoon, D. K. Efetov, P. Kim, S. H. Chun, Nanocrystalline Graphite Growth on Sapphire by Carbon Molecular Beam Epitaxy, J. Phys. Chem. C **115** (2011) 4491-4494. https://doi.org/10.1021/jp110650d
18. J. Kwak, S. Lee, H. Lee, G. Anoop, H. Lee, W. Kim, S. Ryu, H. Kim, J. Jo, Direct growth of nano-crystalline graphite films using pulsed laser deposition with in-situ monitoring based on reflection high-energy electron diffraction technique, Appl. Phys. Lett. **108** (2016) 123107 https://doi.org/10.1063/1.4944845
19. X. Li, W. Dai, Q. Wang, Y. Liang, Z. Wu, Diamond-like/graphite-like carbon composite films deposited by high-power impulse magnetron sputtering, Diam. Relat. Mater. **106** (2020) 107818 https://doi.org/10.1016/j.diamond.2020.107818.
20. M. Huang, X. Zhang, P. Ke, A. Wang, Graphite-like carbon films by high power impulse magnetron sputtering, Appl. Surf. Sci. **283** (2013) 321-326 https://doi.org/10.1016/j.apsusc.2013.06.109.
21. R. Kato, M. Hasegawa, Fast synthesis of thin graphite film with high-performance thermal and electrical properties grown by plasma CVD using polycrystalline nickel foil at low temperature, Carbon **141** (2019) 768-773 https://doi.org/10.1016/j.carbon.2018.09.074.
22. V.A. Krivchenko, A.A. Pilevsky, A.T. Rakhimov, B.V. Seleznev, N.V.

Suetin, M.A. Timofeyev, A.V. Bespalov, and O.L. Golikova, Nanocrystalline graphite: Promising material for high current field emission cathodes, J. Appl. Phys. **107** (2010) 014315 https://doi.org/10.1063/1.3277054

23. V.A. Krivchenko, V.V. Dvorkin, N.N. Dzbanovsky, M.A. Timofeyev, A.S. Stepanov, A.T. Rakhimov, N.V. Suetin, O.Yu. Vilkov, L.V. Yashina, Evolution of carbon film structure during its catalyst-free growth in the plasma of direct current glow discharge, Carbon **50** (2012) 1477-1487 https://doi.org/10.1016/j.carbon.2011.11.018.
24. G. Kalita, M.S. Kayastha, H. Uchida, K. Wakita, M. Umeno, Direct growth of nanographene films by surface wave plasma chemical vapor deposition and their application in photovoltaic devices, RSC Adv. **2** (2012) 3225–3230 https://doi.org/10.1039/C2RA01024K
25. D. Liu, W. Yang, L. Zhang, J. Zhang, J. Meng, R. Yang, G. Zhang, D. Shi, Two-step growth of graphene with separate controlling nucleation and edge growth directly on SiO2 substrates, Carbon **72** (2014) 387-392, https://doi.org/10.1016/j.carbon.2014.02.030.
26. T. Ishijima, H. Toyoda, Y. Takanishi, H. Sugai, Design of Large-Area Surface Wave Plasma Excited by Slotted Waveguide Antennas with Novel Power Divider,Jpn. J. Appl. Phys. **50** (2011) 036002 http://dx.doi.org/10.1143/JJAP.50.036002
27. J. Kim, K. Tsugawa, M. Ishihara, Y. Koga, M. Hasegawa, Large-area

surface wave plasmas using microwave multi-slot antennas for nanocrystalline diamond film deposition, Plasma Sources Sci. Technol. **19** (2009) 015003
http://dx.doi.org/10.1088/0963-0252/19/1/015003

28. J. Kim, M. Ishihara, Y. Koga, K. Tsugawa, M. Hasegawa, S. Iijima, Low-temperature synthesis of large-area graphene-based transparent conductive films using surface wave plasma chemical vapor deposition, Appl. Phys. Lett. **98** (2011) 091502
https://doi.org/10.1063/1.3561747
29. Y. Hotta, H. Toyoda, H. Sugai, High-speed μc-Si films deposition and large-grain poly-Si films deposition by surface wave discharge, Thin Solid Films **515** (2007) 4983-4987
https://doi.org/10.1016/j.tsf.2006.10.053.
30. S. Somiya, H. Toyoda, Y. Hotta, H. Sugai, Suppression of Oxygen Impurity Incorporation into Silicon Films Prepared from Surface-Wave Excited H_2/SiH_4 Plasma, Jpn. J. Appl. Phys. **43** (2004) 7696-7700
https://doi.org/10.1143/JJAP.43.7696
31. L.K. Cheah, X. Shi, B.K. Tay, E. Liu, Modification of tetrahedral amorphous carbon film by concurrent Ar ion bombardment during deposition, Surf. Coat. Technol. **105** (1998) 91-96
https://doi.org/10.1016/S0257-8972(98)00462-9.
32. Y. Wang, L. Wang, G. Zhang, S.C. Wang, R.J.K. Wood, Q. Xue, Effect of bias voltage on microstructure and properties of Ti-doped graphite-like carbon films synthesized by magnetron sputtering, Surf. Coat.

Technol. **205** (2010) 793-800
https://doi.org/10.1016/j.surfcoat.2010.07.112.

33. A.A. Ogwu, R.W. Lamberton, P.D. Maguire and J.A. McLaughlin, The effect of the substrate bias on the Raman spectra and thermal stability of diamond-like carbon (DLC) and silicon-modified DLC films prepared by plasma-enhanced chemical vapour deposition (PECVD) J. Phys. D: Appl. Phys. **32** (1999) 981-987
https://doi.org/10.1088/0022-3727/32/9/306
34. M. A. Tamor, W. C. Vassell, Raman ‘‘fingerprinting’’ of amorphous carbon films, J. Appl. Phys. **76** (1994) 3823-3830
https://doi.org/10.1063/1.357385
35. J. Robertson, Diamond-like amorphous carbon, Mater. Sci. Eng. R Rep. **37** (2002) 129-281
https://doi.org/10.1016/S0927-796X(02)00005-0.
36. A.C. Ferrari and J.Robertson, Interpretation of Raman spectra of disordered and amorphous carbon, Phys. Rev. **61** (2000) 14095 - 14107
https://doi.org/10.1103/PhysRevB.61.14095
37. M. Veres, M. Koós, I. Pócsik, IR study of the formation process of polymeric hydrogenated amorphous carbon film, Diam. Relat. Mater. **11** (2002) 1110-1114,
https://doi.org/10.1016/S0925-9635(02)00011-0.
38. H. Kojima, H. Kako, M. Terada, H. Sugai and T. Okuda, Experimental study on reduction of hydrogen content in low z thin films by controlling DC glow discharge conditions, Jpn. J. Appl. Phys. 24

(1985) 1432-1435
https://doi.org/10.1143/JJAP.24.1432

39. P. J. Fallon, V. S. Veerasamy, C. A. Davis, J. Robertson, G. A. J. Amaratunga, W. I. Milne and J. Koskinen, Properties of filtered-ion-beam-deposited diamondlike carbon as a function of ion energy, Phys. Rev. B **48** (1993) 4777-4782
https://doi.org/10.1103/PhysRevB.48.4777

40. A. Ermolieff, A. Chabli, F. Pierre, G. Rolland, D. Rouchon, C. Vannuffel, C. Vergnaud, J. Baylet and M.N. Séméria, XPS, Raman spectroscopy, X-ray diffraction, specular X-ray reflectivity, transmission electron microscopy and elastic recoil detection analysis of emissive carbon film characterization, Surf. Interface Anal. **31** (2001) 185-190.
https://doi.org/10.1002/sia.955

41. L Ponsonnet, C Donnet, K Varlot, J.M Martin, A Grill, V Patel,EELS analysis of hydrogenated diamond-like carbon films, Thin Solid Films 319 (1998) 97-100.
https://doi.org/10.1016/S0040-6090(97)01094-8

Figure Captions

Fig. 1. Schematic of experimental apparatus.

Fig. 2. Typical (a) voltage and (b) current waveforms of the stage.

Fig. 3. Spatial profiles of (a) plasma density along *z*-axis at *x*=0 and (b) along *x*-axis at *z*=8 cm.

Fig. 4. Spatial uniformities of (a) deposition rate and (b) sheet resistance on the stage.

Fig. 5. Bias voltage dependences of (a) deposition rate and (b) sheet resistance.

Fig. 6. (a) Stage current, (b) deposition rate and (c) sheet resistance as a function of the stage position along *z* axis.

Fig. 7. Bias voltage dependences of (a) Raman spectra, (b) G peak position and (c) *I*(D)/*I*(G) ratio.

Fig. 8. Bias voltage dependences of (a) FT-IR spectra and (b) H content.

Fig. 9. (a) XPS survey data of GLC film (V_B: 2.0 kV). (b) Bias voltage dependence of XPS spectra with C1s peak separation (sp^2, sp^3 and C-O). (c) Bias voltage dependence of sp^2/sp^3 content ratio.

Fig. 10. (a) TEM image of carbon film (V_B = 2.0 kV), (b) EELS spectrum and (c) C_K edge sp^2 mapping.

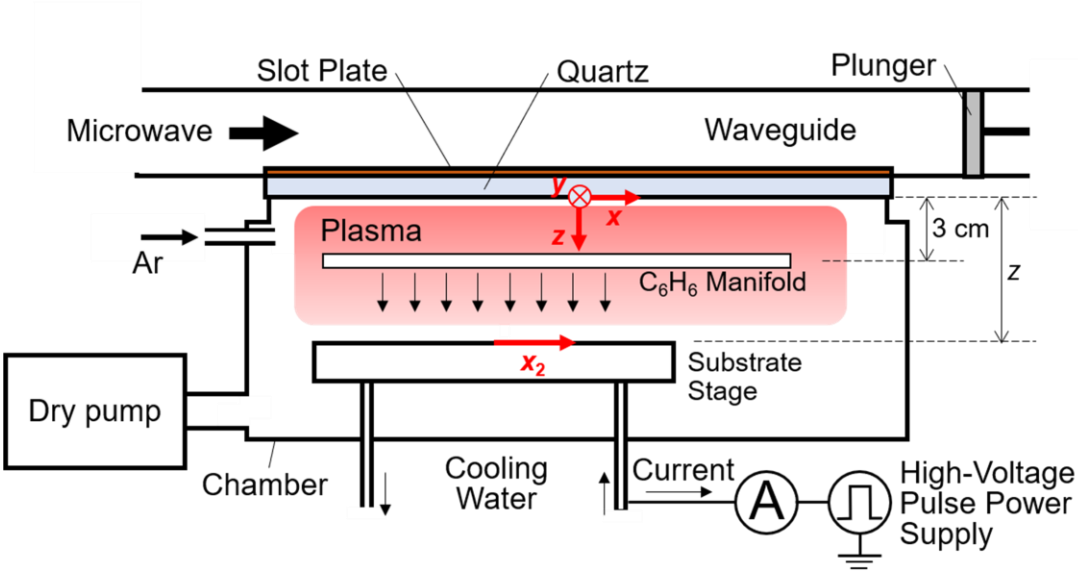

Fig. 1. Schematic of experimental apparatus.

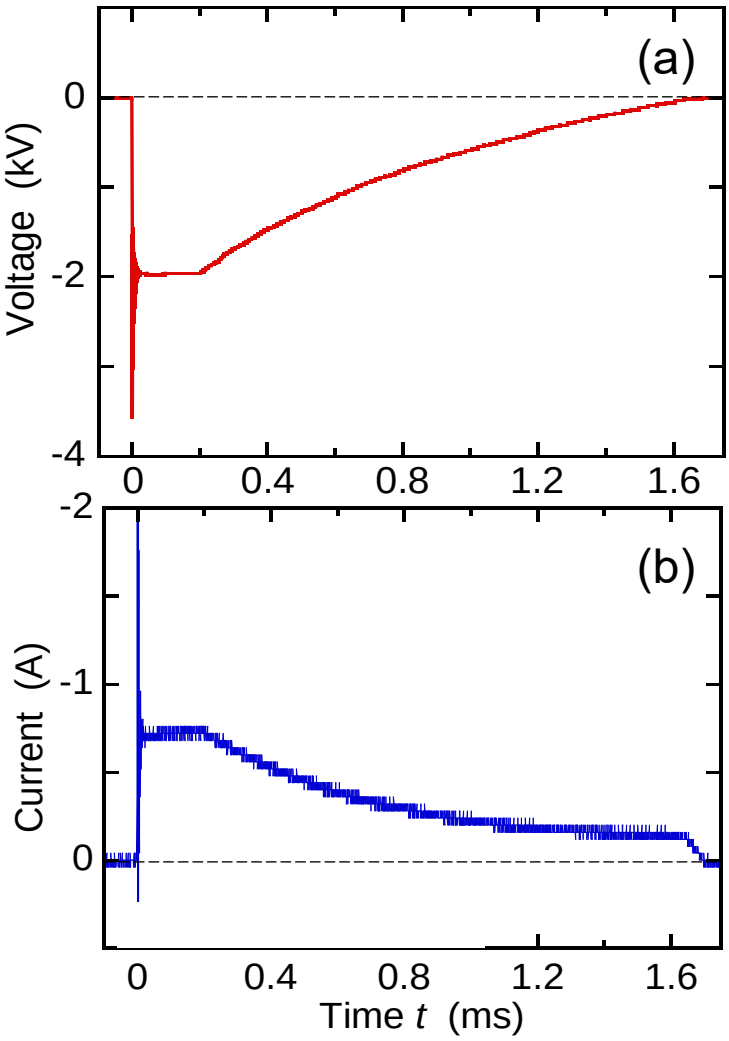

Fig. 2. Typical (a) voltage and (b) current waveforms of the stage.

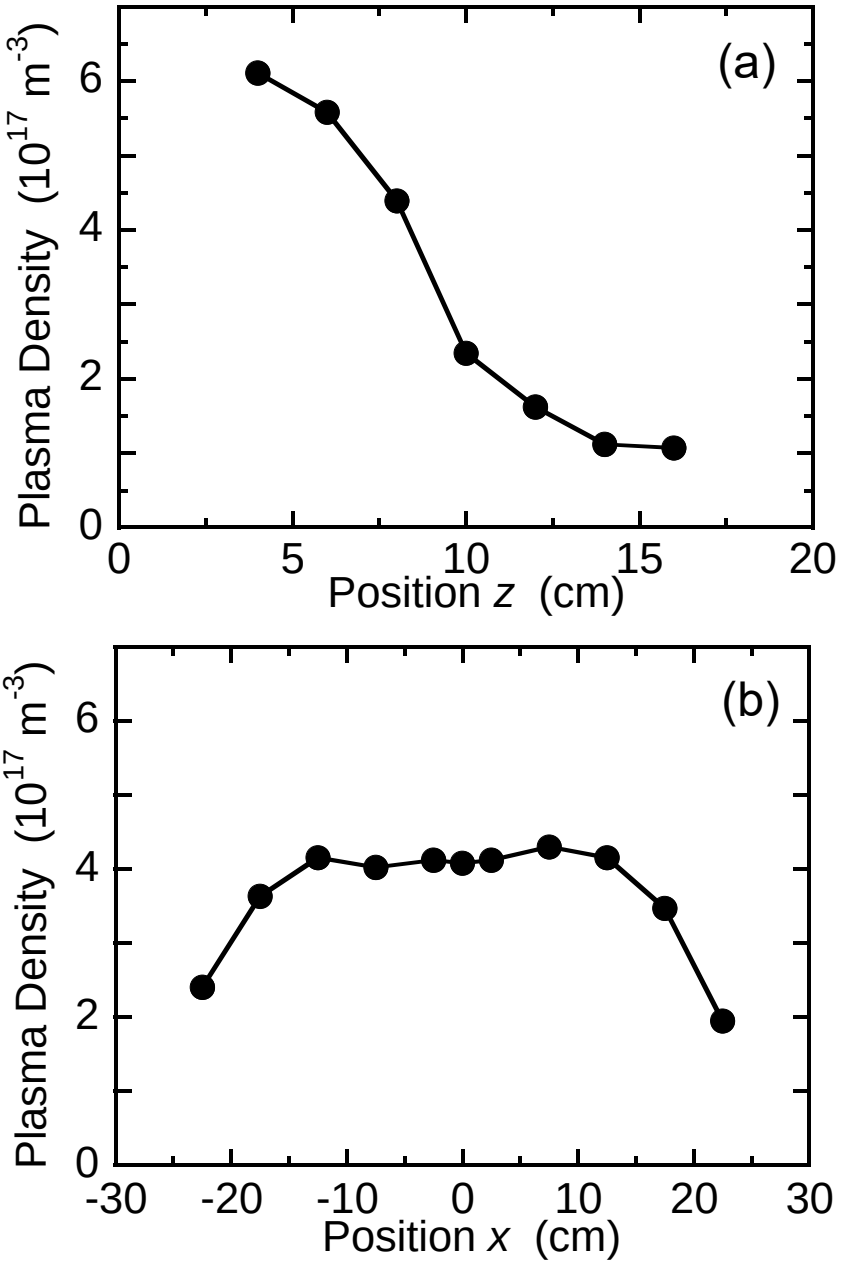

Fig. 3. Spatial profiles of (a) plasma density along z-axis at x=0 and (b) along x-axis at z=8 cm.

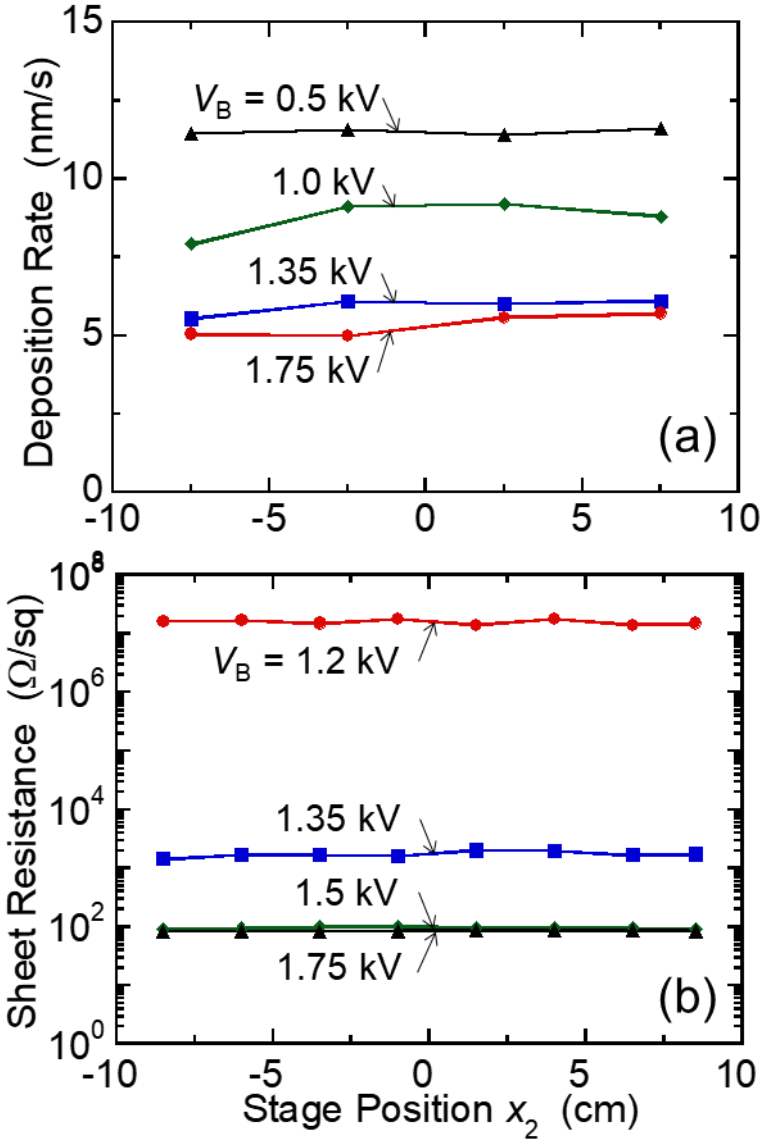

Fig. 4. Spatial uniformities of (a) deposition rate and (b) sheet resistance on the stage.

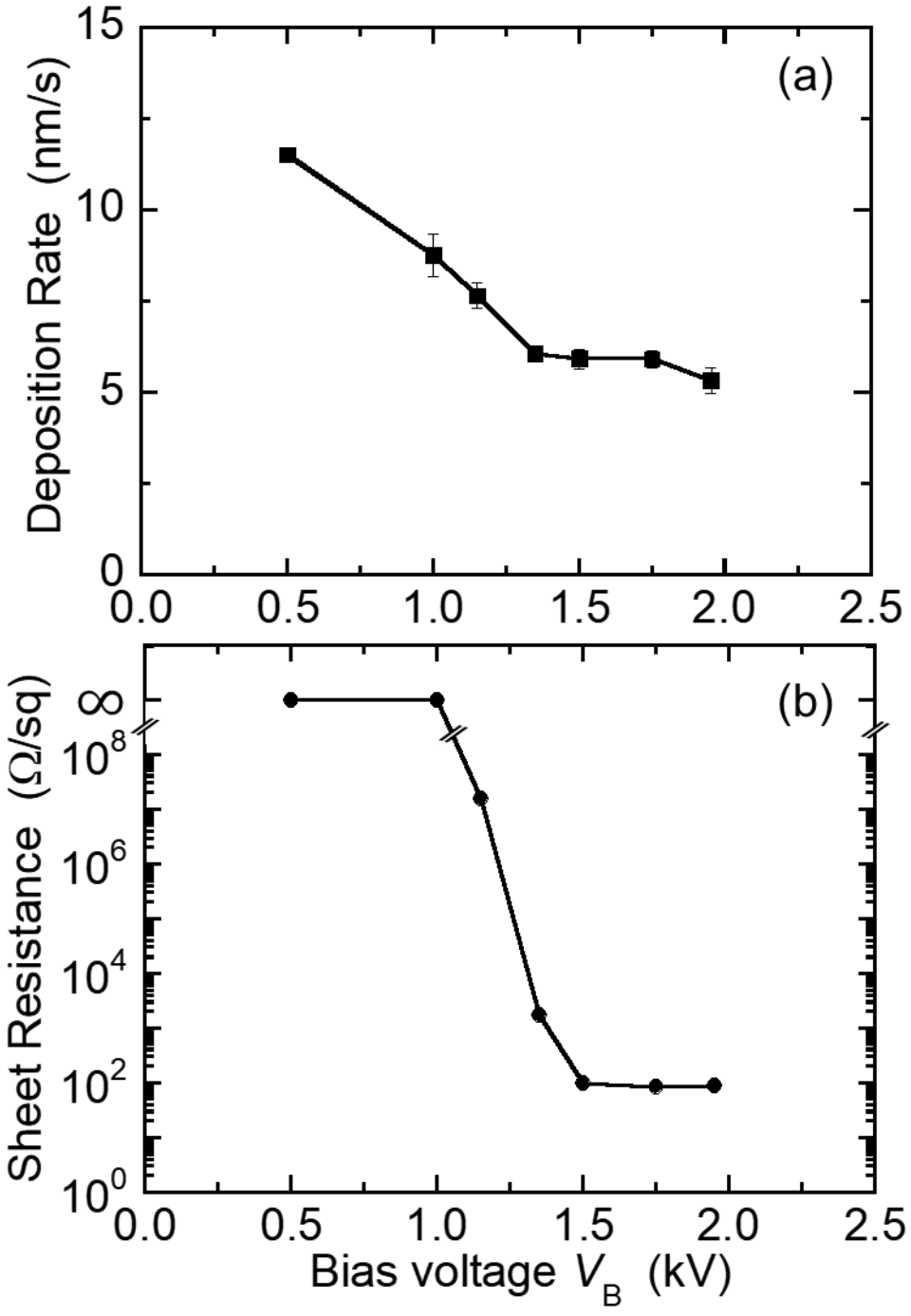

Fig. 5. Bias voltage dependences of (a) deposition rate and (b) sheet resistance.

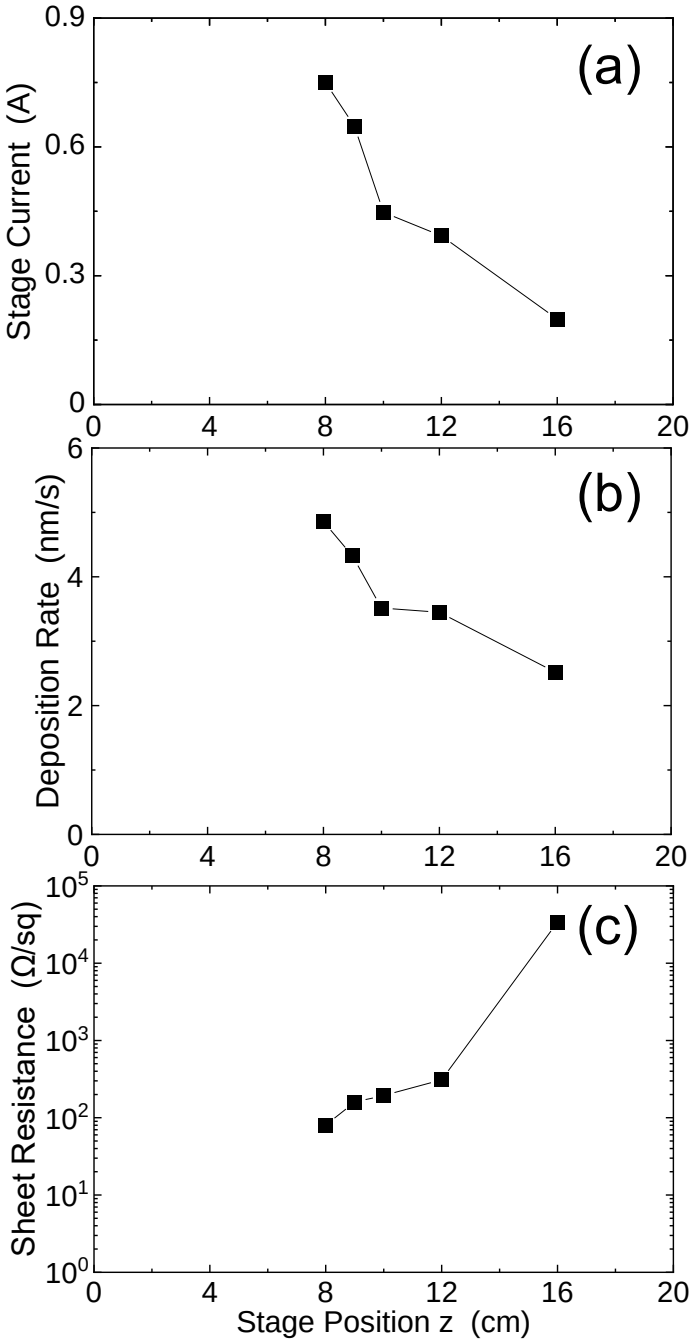

Fig. 6. (a) Stage current, (b) deposition rate and (c) sheet resistance as a function of the stage position along *z* axis.

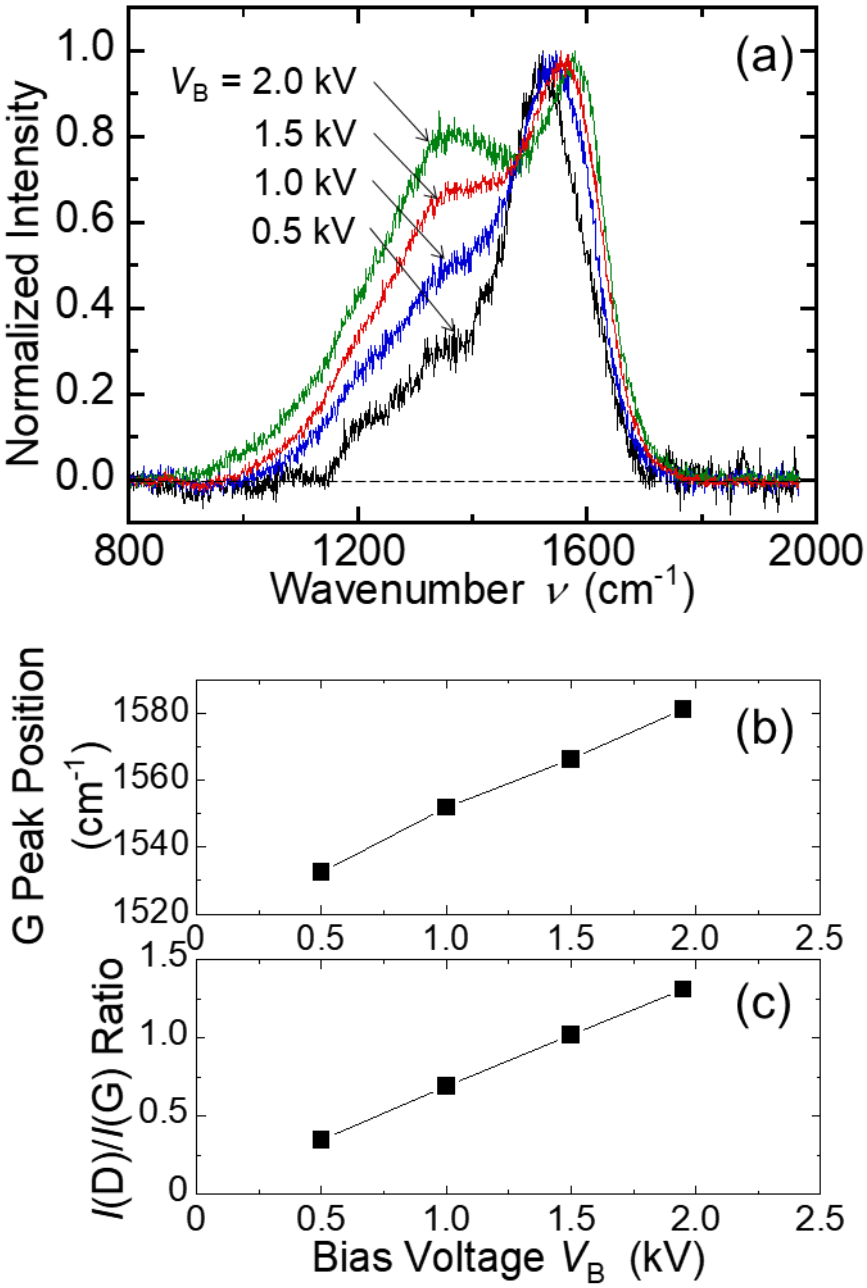

Fig. 7. Bias voltage dependences of (a) Raman spectra, (b) G peak position and (c) I(D)/I(G) ratio.

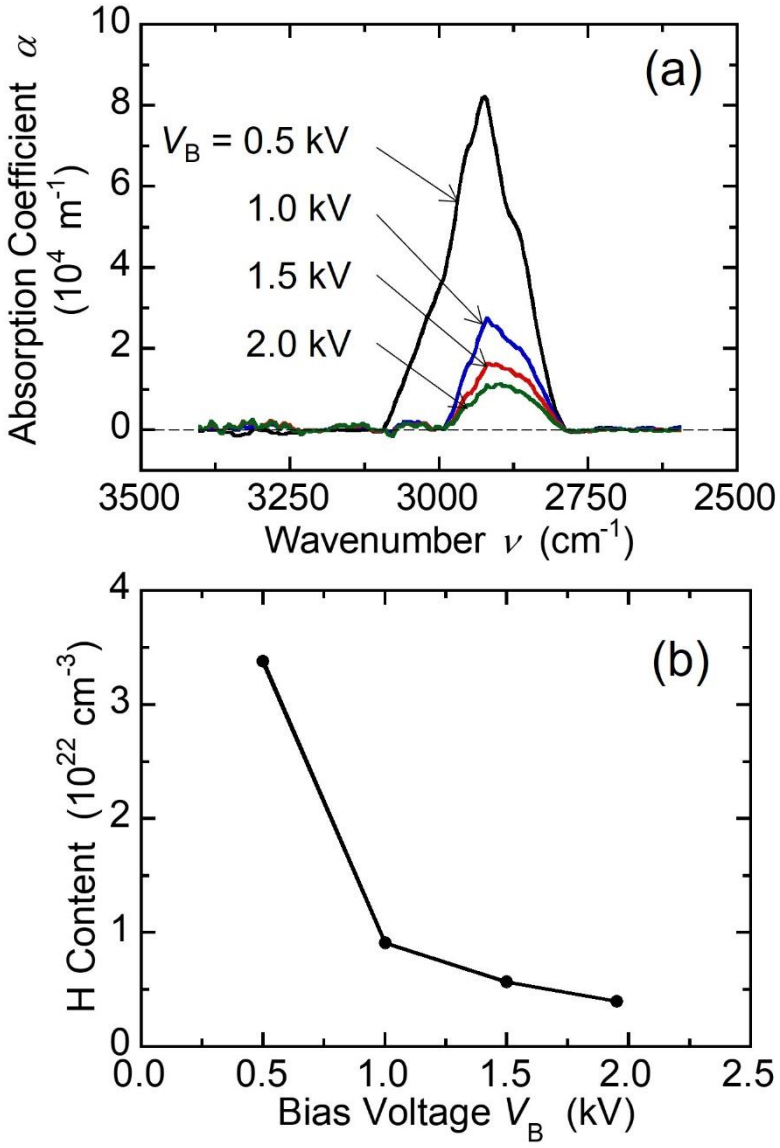

Fig. 8. Bias voltage dependences of (a) FT-IR spectra and (b) H content.

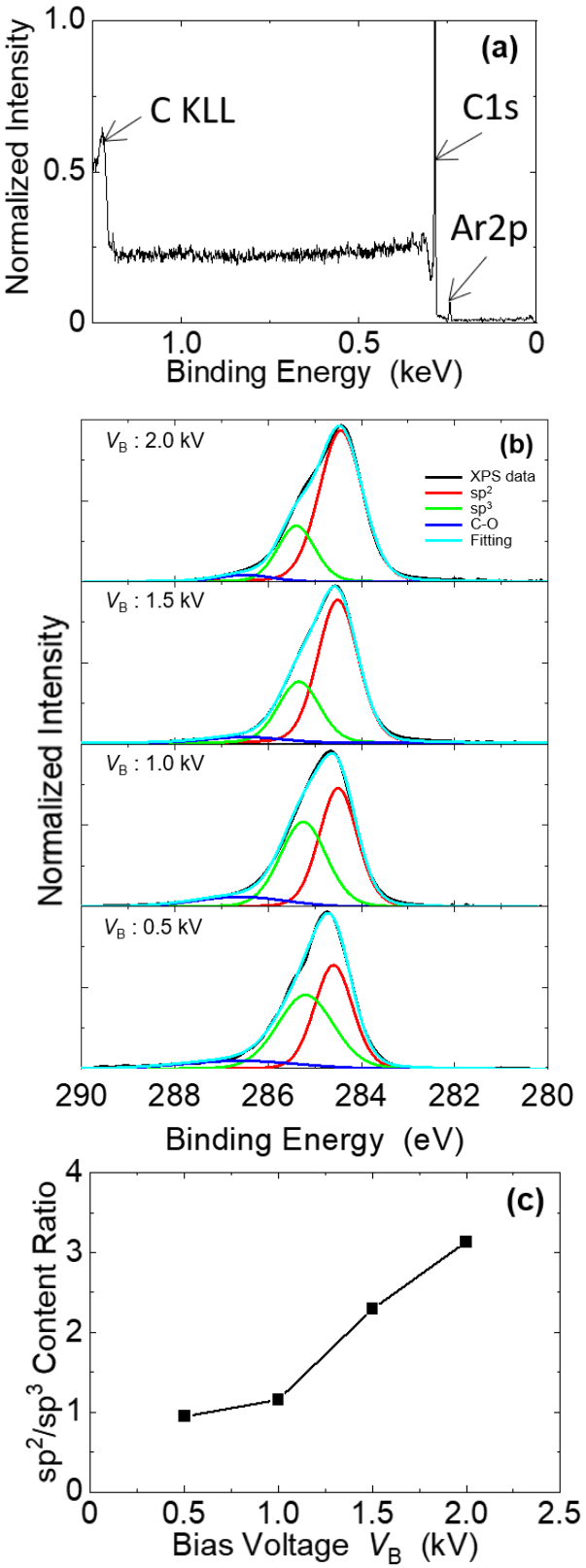

Fig. 9. (a) XPS survey data of GLC film (V_B: 2.0 kV). (b) Bias voltage dependence of XPS spectra with C1s peak separation (sp^2, sp^3 and C-O). (c) Bias voltage dependence of sp^2/sp^3 content ratio.

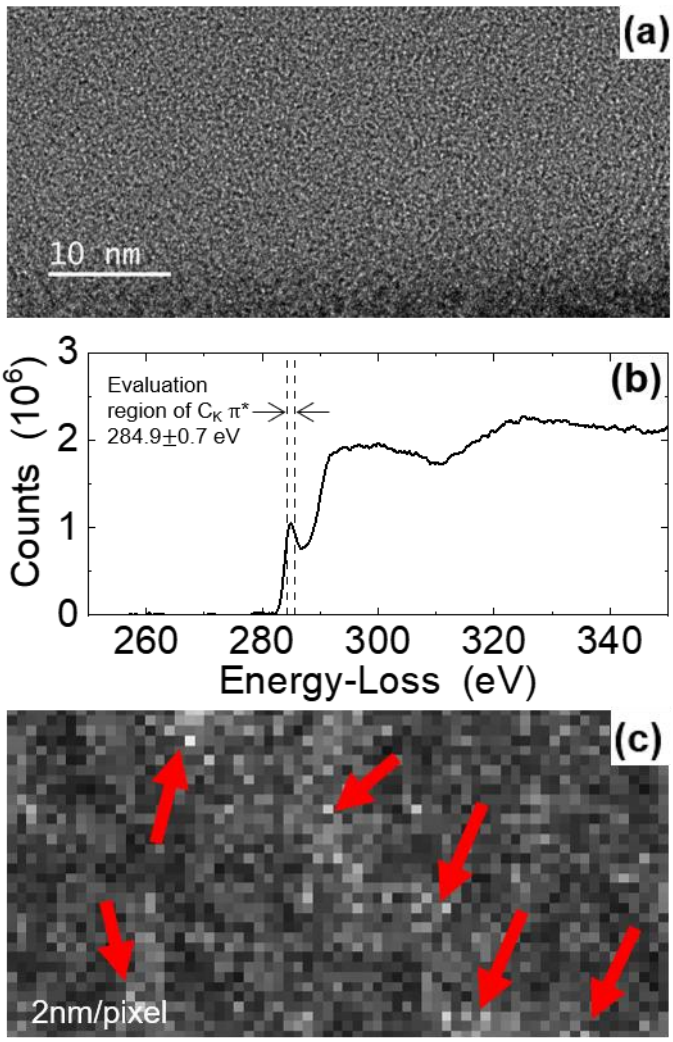

Fig. 10. (a) TEM image of carbon film (V_B = 2.0 kV), (b) EELS spectrum and (c) C_K edge sp^2 mapping.